

pubs.acs.org/JPCC Article

Origin of Kinetic Dispersion in Eosin-Sensitized TiO₂: Insights from Single-Molecule Spectroscopy

Kelly M. Kopera, Harrison G. Tuckman, Grayson R. Hoy, and Kristin L. Wustholz*



Cite This: J. Phys. Chem. C 2021, 125, 23634–23645



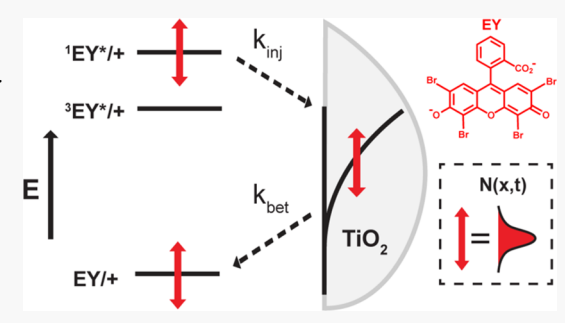
ACCESS

Metrics & More

Article Recommendations

3 Supporting Information

ABSTRACT: By removing the effects of ensemble averaging and molecular aggregation, we untangle the factors that govern the dispersive electron transfer kinetics of eosin-sensitized TiO₂, focusing on the impact of environmental heterogeneity versus injection from multiple excited states. The blinking dynamics of single eosin Y chromophores on nanocrystalline TiO₂ films are analyzed using a change point detection algorithm for binned data. Robust statistical analysis based on maximum likelihood estimation, Kolmogorov–Smirnov tests, and log likelihood ratio tests is used to determine the functional form that best fits the resulting on- and off-time distributions and to distinguish between mechanisms for dispersive electron transfer. Using this approach, we find that the on- and off-time distributions



for eosin Y on TiO₂ are best fit to lognormal distributions corresponding to $\mu_{\rm on} = -0.64 \pm 0.04$, $\sigma_{\rm on} = 1.52 \pm 0.02$, $\mu_{\rm off} = -0.23 \pm 0.04$, and $\sigma_{\rm off} = 1.96 \pm 0.03$, respectively. Monte Carlo simulations based on the Albery model for dispersive electron transfer (i.e., where the median rate constant κ is modified by the exponential of a parameter, κ , that is normally distributed, $\kappa = \kappa e^{-\gamma \kappa}$ successfully reproduce this behavior using a median rate constant for injection and back electron transfer of ~10¹⁰ and ~10⁴ s⁻¹, respectively, and a corresponding energetic dispersion, κ , of ~200–350 meV. To examine how injection from both the singlet and triplet excited states contributes to this dispersion, we studied two rhodamine sensitizers, R123 and SROX, that inject only from their singlet excited state. Surprisingly, when access to the T₁ state is minimized in going from EY to R123 and SROX, kinetic dispersion actually increases. Collectively, these observations support the interpretation that static and dynamic inhomogeneities at the EY–TiO₂ interface govern kinetic dispersion, with dynamic fluctuations in binding configuration and/or vibrational motion playing a decisive role.

INTRODUCTION

The need for clean, renewable energy sources is increasingly vital with rising global energy consumption and growing concerns over climate change. Dye-sensitized solar cells (DSSCs), comprising mesoporous thin films of nanocrystalline TiO₂ sensitized with molecular chromophores, have tremendous potential to address these concerns by inexpensively converting sunlight into electricity. In DSSCs, upon photoexcitation of the sensitizer with visible light, electrons are injected from the molecular excited state into the conduction band or energetically accessible trap states of TiO₂. Dyes are then regenerated by electron donation from an electrolyte or through back electron transfer (BET) from the semiconductor. Electron injection at the dye—semiconductor interface has also been exploited for chemical fuel generation in dye-sensitized photoelectrochemical cells (DSPECs). 3-6

Because solar energy conversion efficiency in these devices is dependent on the electron transfer processes between the dye and the semiconductor, there is a substantial literature precedent for time-resolved spectroscopy studies of the injection and BET kinetics in dye-sensitized ${\rm TiO_2}^{.7-11}$ Numerous mechanistic studies have shown that while injection typically occurs on picosecond timescales and unwanted BET

to repopulate the molecular ground state is relatively slow, the reported kinetics are remarkably heterogeneous, varying by several orders of magnitude in time. This kinetic heterogeneity, sometimes termed "stretched exponential", "multiphasic", or simply "dispersive" kinetics, is often attributed to environmental heterogeneity in TiO₂ 12,13,16-19 and more recently competition between excited-state relaxation and injection from within the same manifold of dye excited states. However, the extent and origin of kinetic dispersion are difficult to determine using ensemble-averaged spectroscopic methods alone, which are complicated not only by averaging but also by the presence of molecular aggregates. Remarkably heterogeneous, varying by several contents and time.

Several studies have shown that single-molecule blinking measurements can probe the full distribution of electron

Received: August 27, 2021 Revised: October 1, 2021 Published: October 26, 2021





transfer behavior occurring at dye-semiconductor interfaces. 21-28 Blinking is characterized as fluctuations in emissive intensities that occur during continuous photoexcitation due to the population and depopulation of optically bright and dark vibronic states, respectively. For example, if blinking occurs through a low-lying triplet state (T_1) , then these processes obey first-order kinetics and the emissive and non-emissive event durations (i.e., "on" and "off" times, respectively) are fit to exponential functions to extract the rate constants for intersystem crossing from the singlet excited state (S_1) to T_1 and decay to the singlet ground state (S₀). In the case of photoinduced electron transfer, the on- and off-time distributions are related to the injection and BET kinetics, respectively. Previous single-molecule studies have confirmed that electron transfer kinetics at the dye-TiO2 interface are not first-order. However, the functional form of the on- and off-time distributions, and therefore the origin of dispersive kinetics, remains a point of debate.

For example, the photophysical distributions of coumarin 343 and cresyl violet, ^{21,22} Atto647N, ²⁹ a Zn porphyrin, ³⁰ and a Ru(II) polypyridyl complex ^{31,32} on TiO₂ have been reported to follow power laws, consistent with a mechanism in which the rate constants for injection (k_{inj}) and BET (k_{BET}) vary due to an exponential distribution of activation energies to photoinduced electron transfer.³¹ Chen and Marcus also proposed a reaction-diffusion mechanism to explain the observation of power laws.³³ However, others have questioned the essentially ubiquitous application of power laws to blinking data.^{24,25,34-36} For example, we demonstrated that while the on- and off-time distributions of rhodamine-sensitized TiO2 appear to follow power laws, they are actually best fit to lognormal distributions. ^{24,25} The observation of lognormal distributions is consistent with the Albery model for dispersive kinetics where the activation barriers to electron transfer are normally distributed.³⁷ In both the power law and Albery models, the dispersive kinetics at the dye-TiO2 interface is typically attributed to environmental heterogeneity across the sample: local variations in radii or surface charge of the TiO₂ colloid that impact the relative energetics between the dye states and the density of TiO2 states. However, there is some evidence to suggest that not all kinetic dispersion has environmental origins. Zigler et al. used transient absorption spectroscopy to show that Ru polypyridyl complexes exhibit significant kinetic heterogeneity due to slow injection from the thermally equilibrated excited state and fast injection from higher energy states within the dye excited-state manifold.²⁰ The extent to which injection from multiple dye excited states (e.g., S_1 and T_1) contributes to kinetic dispersion has not been investigated at the molecular level. In this study, we examine how environmental heterogeneity and injection from multiple excited states contribute to kinetic dispersion using a combination of single-molecule blinking measurements, robust statistical analysis to identify the functional form of the distributions, and Monte Carlo simulations.

The organic dye sensitizer eosin Y (EY) has been utilized in DSSCs and several photocatalytic systems for $\rm H_2$ generation. Has been utilized in the system crossing from $\rm S_1$ to $\rm T_1$ (i.e., $k_{\rm isc}=8.4\times10^8~\rm s^{-1}$ in $\rm H_2O$), and prior work has shown that injection to $\rm TiO_2$ from both excited states is energetically feasible. Figure 1 presents the exponentially distributed density of $\rm TiO_2$ states, g(E), 10,13,43,44 alongside the redox potentials of the singlet and triplet excited states of EY (i.e., $^{1}\rm EY^{*/+} = -1.26~\rm V$ and $^{3}\rm EY^{*/+}$

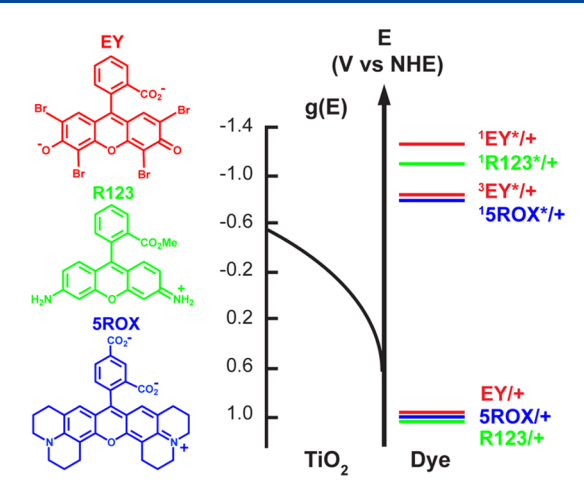


Figure 1. Density of states, g(E), of TiO_2 with the indicated redox states of the sensitizers employed in this study: EY, rhodamine 123 (R123), and 5-carboxy-X-rhodamine (5ROX).

= -0.86 V vs NHE, respectively). 39,45,46 Previous timeresolved spectroscopy studies by Grätzel and co-workers demonstrated that injection from EY to TiO_2 is multiphasic, with the fastest component estimated to occur with a k_{inj} of 3.8 \times 10^{12} s⁻¹. 39,45 Although these studies revealed the injection kinetics of EY-sensitized TiO_2 to be dispersive and predominately occur from S₁, they are complicated by the presence of molecular aggregates and ensemble averaging. The extent to which rare T_1 injection events contribute to this kinetic dispersion is unknown.

Here, we use single-molecule blinking measurements to probe the full extent and origin(s) of kinetic dispersion at the EY-TiO₂ interface. Robust statistical analysis determines the functional forms of the photophysical distributions, and Monte Carlo simulations based on a simple physical model successfully reproduce the empirical data. By examining EY alongside other xanthylium sensitizers (i.e., R123 and 5ROX, Figure 1) that do not possess heavy atoms and inject from just S_1 , we elucidate the impact of multiple injection pathways (i.e., from S_1 and T_1) on kinetic dispersion. In doing so, we disentangle the role of environmental and photophysical heterogeneity in kinetic dispersion, showing that the electron transfer kinetics of EY are less dispersive relative to R123 and 5ROX. We discuss the possible origins of this behavior in the context of Marcus-Gerischer theory for interfacial electron transfer.

METHODS

Materials and Sample Preparation. EY (~99%), R123 (99+%), and 5ROX (triethylammonium salt) were used as received from Sigma-Aldrich, Acros Organics, and Thermo Fisher Scientific, respectively. Ethanol (absolute anhydrous, 200 proof) was obtained from Pharmco-Aaaper. EY solutions were prepared in ethanol using a base-bathed glassware. Corresponding R123 and 5ROX solutions were made in ultrapure water (Thermo Scientific, EasyPure II, 18.2 MΩ cm). Glass coverslips (Fisher Scientific, 12-545-102) were cleaned in a base bath for 12–24 h, rinsed in ultrapure water, and dried using clean air (Wilkerson, X06-02-000). For single-molecule measurements on glass, samples were prepared by spin-coating $35 \,\mu$ L of a 5×10^{-10} M EY solution onto a clean glass coverslip using a spin coater (Laurell Technologies, WS-400-6NPP-LITE) operating at 3000 rpm. Corresponding TiO₂ samples

were prepared by diluting nanocrystalline TiO_2 (Solaronix, Ti-Nanoxide HT-L-SC, 7% wt 15–20 nm anatase particles) to ~1 g/L in ultrapure water and spin-coating three 100 μ L aliquots of the resulting solution onto a clean glass coverslip at 3000 rpm. The coverslip was sintered in a muffle furnace (Thermo Scientific, Thermolyne) set to 500 °C for 30 min to remove impurities and produce a sub-micron thick mesoporous film, as specified by the manufacturer. Then, 35 μ L of a 5 × 10⁻¹⁰ M dye solution was spun-coat onto the sintered TiO_2 substrate. The resulting single-molecule samples were mounted in a custom designed flow cell and flushed with N_2 (Airgas, 100%) at a rate of 0.2–0.5 scfh (Key Instruments, MR3A01AVVT).

Single-Molecule Confocal Microscopy. Samples for single-molecule studies were placed on a nanopositioning stage (Physik Instrumente, LP E-545) on an inverted confocal microscope (Nikon, TiU). Laser excitation at 532 nm (Spectra Physics, Excelsior) was focused to a diffraction-limited spot using a high numerical aperture (NA) 100× oil-immersion objective (Nikon Plan Fluor, NA = 1.3). Excitation powers $(P_{\rm exc})$ of 0.37, 23, and 5 μW at the sample were used for singlemolecule measurements of EY on glass, EY on TiO2, and R123/5ROX on TiO2, respectively. These excitation powers were selected to optimize the emission signal of single molecules while minimizing rapid photobleaching. Emission from the sample was collected through the objective, passed through an edge filter (Semrock, LP03-532RS-2S), and focused to an avalanche photodiode detector with a 50 μ m aperture (MPD, PDM050CTB) to provide confocal resolution. A z-axis microscope lock (Applied Science Instruments, MFC-2000) was used to maintain focus during raster scans. A custom LabView program was used to control the nanopositioning stage and collect the corresponding emission intensity using a 30 ms dwell time. The observation of diffraction-limited spots, blinking dynamics, irreversible singlestep photobleaching, and concentration dependence of the spot density in control experiments on glass (i.e., ~5-10 molecules per 36 μ m² for 5 × 10⁻¹⁰ M EY on glass) were used to establish single-molecule detection. Single-molecule blinking dynamics were acquired using a 10 ms integration time for 200

Change Point Detection and Fitting. A change point detection (CPD) method was used to analyze blinking dynamics and parse the trajectories into statistically-significant intensities and corresponding temporal durations. This CPD algorithm largely follows the prescription outlined by Watkins and Yang 47,48 where the locations of the intensity change points are determined recursively via a generalized likelihood ratio test and then clustered together to form the true number of states. However, our method makes a subtle, yet important, differentiation in the critical values used to detect change points. Yang's original CPD method was developed for detecting change points from a series of individual photon arrival times and not binned data. To address this issue, we utilize the derivation by Boudjellaba et al. 49 to calculate critical values and detect change points for binned data (the table of critical values is available in the Supporting Information). This derivation provides a recursive procedure by which the critical values are calculated for a given number of photons and number of bins. Comparison of the CPD algorithms for individual photon arrival times versus binned data at a 90% confidence interval demonstrates that the methods produce essentially the same result at low photon counts per bin (i.e., when the data are near the limit of individual photon arrival

times). However, as the number of photons per bin is increased, the original CPD method increasingly exceeds the expected 90% confidence interval such that some change points are not detected (see Figure S1, Supporting Information).

The resulting CPD algorithm for binned data was applied to experimental and simulated blinking traces. The first and last events are eliminated since they are artificially set by the observation period. The lowest deconvolved intensity level is designated as a non-emissive (off), and levels with intensities greater than 1 standard deviation above the rms noise are denoted as emissive (on). Blinking events are further parsed into two categories: segments and intervals. A segment corresponds to the duration of an event at a particular intensity. An interval is the duration of successive segments that occur prior to a switch between on and off (i.e., intervals are generally longer than segments). Since on and off intervals are directly related to dark-state production and decay corresponding to electron transfer, they are the focus of this study and simply referred to as on and off times hereafter. All fitting procedures and Monte Carlo simulations were completed in MATLAB (version R2019a) and C. Consistent with prior work, the log-likelihood ratio (LLR) and associated $p\text{-value}\ (p_{\mathcal{R}})$ are calculated according to the Vuong method using R (version 3.3.0). The $p_{\mathcal{R}}$ values were \ll 0.1, indicating that the LLR test is a reliable indicator of which model is a better fit to the data.

■ RESULTS AND DISCUSSION

Blinking Statistics of EY on TiO₂. A confocal microscope employing continuous laser excitation at 532 nm was used to measure the blinking dynamics and probe kinetic dispersion in EY-sensitized TiO₂. Figure 2a,b shows representative false-

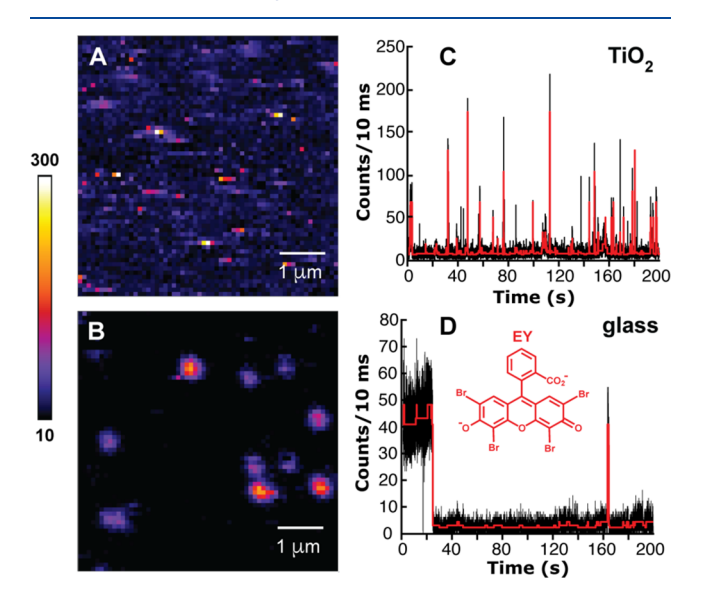


Figure 2. False-colored $6 \times 6 \ \mu m^2$ images of the emission from 5×10^{-10} M EY on (A) TiO_2 and (B) glass, obtained using 532 nm excitation and $P_{\rm exc}$ of 23 and 0.37 μ W, respectively. The color scale corresponds to counts per 30 ms bin. The emission is more pixelated and less intense on TiO_2 , consistent with electron injection to the semiconductor. Blinking dynamics for an individual EY molecule on (C) TiO_2 and (D) glass, recorded using a 10 ms bin time, shown in black. (red) CPD analysis is used to determine statistically significant intensities and event durations.

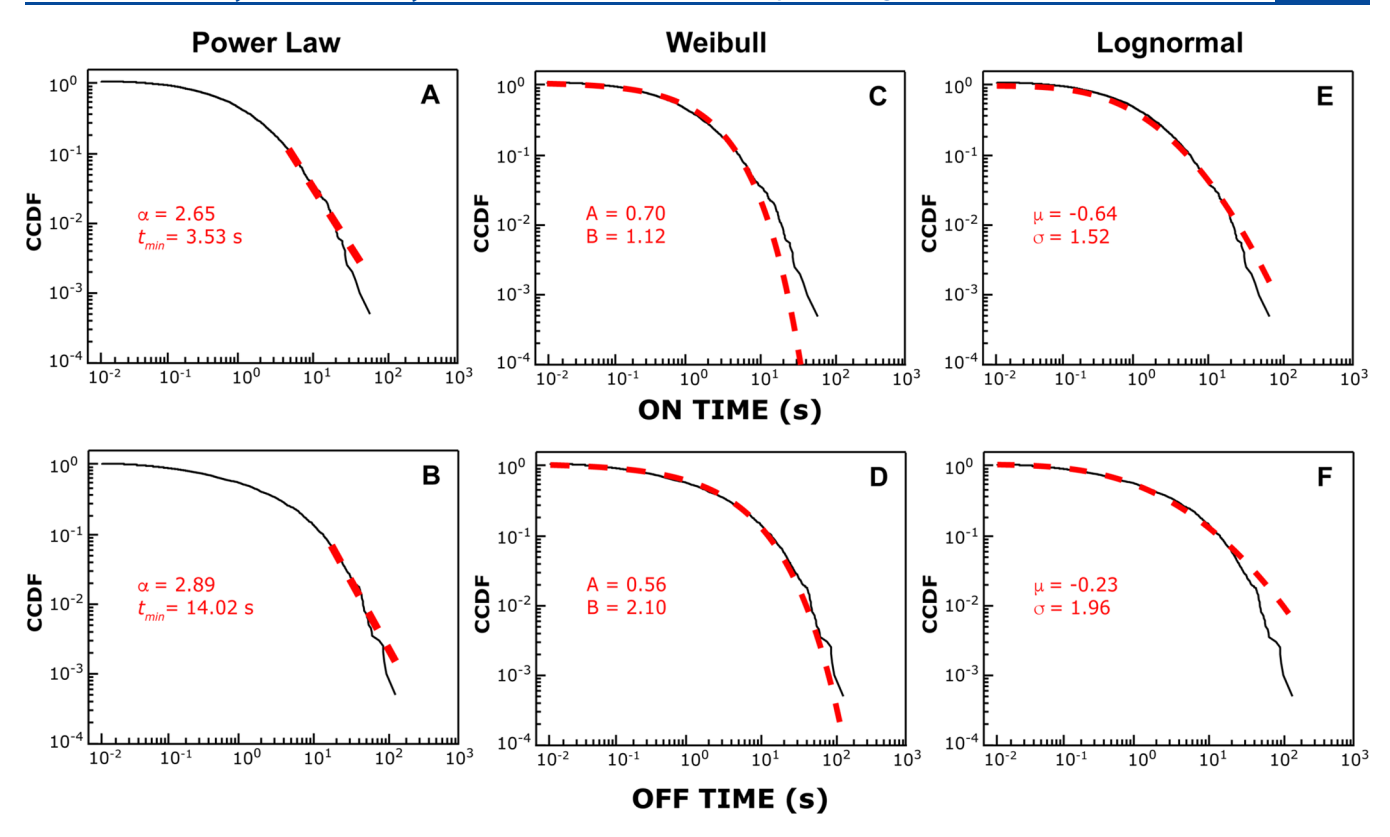


Figure 3. Best fits of the (top) on- and (bottom) off-time CCDFs for 62 molecules of EY on TiO_2 to (A,B) power law, (C,D) Weibull, and (E,F) lognormal distributions. Fits are shown in red dashed lines. Power-law fits apply to <10% of the data. The Weibull and lognormal CCDFs better represent the entire data set but deviate at long times (>10 s).

colored images of the emission from 5 \times 10^{-10} M EY on nanocrystalline $\rm TiO_2$ and an insulating glass substrate, respectively. The emission intensity of EY is substantially reduced on $\rm TiO_2$ relative to glass (i.e., $\sim \! 1$ vs $\sim \! \! 25$ counts $\mu \rm W^{-1}$), and the corresponding image is substantially more pixelated. These observations are consistent with molecules undergoing frequent excursions to a non-emissive state (i.e., via injection to $\rm TiO_2$) with durations that exceed the 30 ms bin time of the experiment.

The blinking dynamics of EY on TiO₂ are characterized by short bursts of emission (i.e., on times < 100 ms) that are interspersed with longer off times (Figure 2c). Previous studies have shown that applying a simple threshold to quantify the emissive and non-emissive events is problematic. 24,29,51-53 Therefore, blinking dynamics are analyzed using a CPD method that we adapted for binned data. 47-49 CPD analysis of the molecule in Figure 2c reveals 12 distinct intensity levels, including 38 on events and 37 off events, and an event frequency (v_{event}) , defined as the number of on and off events per second of 0.375 s⁻¹. For this molecule, on times (t_{on}) ranging from 20 ms to 13.47 s and off times ($t_{\rm off}$) from 10 ms to 12.22 s are observed. These $t_{\rm off}$ are much longer than the reported T_1 lifetime of EY (i.e., 55 μ s in water, 54 3.6 ms in polymethyl methacrylate, 55 and 1 ms on alumina 56), suggesting that another dark state is operative. The blinking dynamics of EY on glass, which has been attributed to electron transfer to trap states,⁵⁷ is quite different—with molecules exhibiting longer $t_{\rm on}$ and smaller $v_{\rm event}$ on glass as compared to TiO₂. For example, the molecule shown in Figure 2d exhibits 10 distinct intensities, including six on and six off events and an v_{event} of 0.070 s^{-1} . The corresponding t_{on} range from 150 ms to 23.43 s

and $t_{\rm off}$ values span from 70 ms to 131.02 s. The observation that the blinking dynamics of EY demonstrate multiple emissive intensities is consistent with prior single-molecule studies of xanthene and anthraquinone dyes on glass ^{50,57} and TiO₂, ^{24,25} which has been attributed to dynamic fluctuations in excitation, emission, and/or non-radiative decay. Overall, the substrate-dependent emission behavior of EY is consistent with a blinking mechanism that involves injection to TiO₂ to populate a non-emissive radical cation state of the dye.

To establish the physical mechanism responsible for blinking and probe the extent of kinetic dispersion, the on- and off-time distributions for a collection of molecules are measured and fit to various functional forms. Blinking dynamics of 62 molecules of EY on TiO₂ were measured, analyzed with CPD, and collected into on- and off-time distributions, which included a total of 2075 on events and 2057 off events. The average event frequency, $\langle v_{\text{event}} \rangle$, is $0.3 \pm 0.2 \text{ s}^{-1}$ molecule⁻¹, where the error corresponds to the standard deviation from the mean. Individual t_{on} range from 10 ms to 45.43 s, with an average on time, $\langle t_{\rm on} \rangle$, of 2 \pm 1 s. Corresponding $t_{\rm off}$ from 10 ms to 105.92 s are observed, with an average value of 10 \pm 10 s. Consistent with prior studies, the raw on- and off-time distributions are converted into complementary cumulative distribution functions (CCDFs), which describe the probability of an event occurring in a time greater than or equal to taccording to: CCDF = $1 - 1/N\sum_i t_i \le t^{24,34,50,58}$ Figure 3a-f presents the resulting on- and off-time CCDFs of EY on TiO2 on log-log axes, which are broad, heavy tailed, and not well represented by single exponential functions. The observation of dispersive kinetics in EY-sensitized TiO2 motivated us to consider more complex photophysics and corresponding test

Table 1. Best-Fit Parameters and p-Values for Power Law, Weibull, and Lognormal Distributions^a

	power law:			weibull:			lognormal:			
	$\frac{\alpha - 1}{t_{\min}} \left(\frac{t}{t_{\min}}\right)^{-\alpha}$			$\frac{A}{B} \left(\frac{t}{B}\right)^{A-1} e^{(t/B)^A}$			$\frac{1}{t\sigma\sqrt{2\pi}} \mathrm{e}^{-(\ln(t)-\mu)^2/2\sigma^2}$			
	t_{\min} (s)	α	p	A	В	p	μ	σ	p	
ON	3.53	2.65 ± 0.04	0.059	0.700 ± 0.004	1.12 ± 0.03	0	-0.64 ± 0.04	1.52 ± 0.02	0.0050	
OFF	14.02	2.89 ± 0.04	0.021	0.560 ± 0.004	2.10 ± 0.06	0	-0.23 ± 0.04	1.96 ± 0.03	0	
^a Errors represent 1 standard deviation.										

functions such as the power law. To identify the functional form(s) of the data, we apply a statistically principled method based on maximum likelihood estimation (MLE) and the Kolmogorov–Smirnov (KS) test. This approach provides accurate estimates of the best-fit parameters and quantifies the goodness-of-fits of the experimental CCDFs relative to several proposed heavy-tailed functions (i.e., power law, Weibull, and lognormal) using MLE and the KS statistic (i.e., p-value). The probability that the data match the hypothetical model is increased as p approaches unity.

The results of the combined MLE/KS analysis on the onand off-time CCDFs for EY on TiO₂ are shown in Figure 3a-f and Table 1. For both the on- and off-time distributions, power laws yield non-zero p values, but the onset times for power-law behavior (t_{min}) are so late that they leave most of the data unaccounted for. For instance, the off-time CCDF for EY on TiO_2 is best fit to a power law (p = 0.059), but the power law is operative only after a t_{min} of 14.02 s, revealing that the fit only applies to ~7% of the data (Figure 3b). Therefore, power law fits are noted for completeness but not regarded as a good description of the photophysical behavior of EY on TiO₂. These observations are consistent with previous studies that find power laws to be poor representations of on- and off-time CCDFs of rhodamines on glass and TiO₂ substrates, ^{24,25} xanthylium dyes in potassium acid phthalate crystals, 51,53 and anthraquinones on glass.⁵⁰

Although Figure 3c-f demonstrates that the on- and offtime CCDFs are qualitatively well represented by Weibull and lognormal distributions, MLE/KS analysis produced p-values that are close to zero. In cases where the p-value is insufficient to determine the best fit between the empirical data and a hypothesized model, the LLR test has been used to distinguish between two candidate fits.⁵⁹ For example, LLR tests were used to establish the functional form of the on- and off-time CCDFs of alizarin and purpurin on glass.⁵⁰ In this approach, the logarithm of the ratio of two likelihoods (R) will be positive or negative depending on which distribution is a better fit or zero in the event of a tie. When we tested the Weibull distribution as the null hypothesis against the lognormal distribution for both the on- and off-time CCDFs, the resulting negative \mathcal{R} values of -179.8 and -145.6 demonstrate that the lognormal distribution is a better alternative to the Weibull distribution. Thus, the combination of the MLE/KS method and LLR tests demonstrates that the on- and off-time CCDFs of EY on TiO₂ are best described by lognormal distributions. The on-time CCDF for EY on TiO2 is best fit to a lognormal distribution corresponding to $\mu_{\rm on}$ = -0.64 ± 0.04 and $\sigma_{\rm on}$ = 1.52 ± 0.02 where the fit parameters are related to the median and standard deviation of the distribution, respectively. The corresponding off-time CCDF is best fit to a lognormal distribution with $\mu_{\rm off}$ = -0.23 ± 0.04 and $\sigma_{\rm off}$ = 1.96 ± 0.03 .

The on- and off-time CCDFs of EY are appreciably modified on glass relative to the semiconductor substrate. Both data sets are well represented by lognormal distributions (Figure 4a,b),

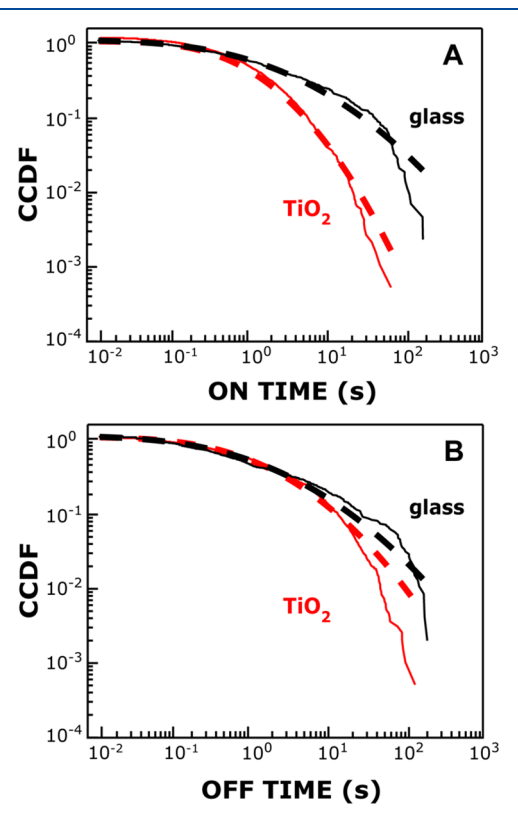


Figure 4. (A) On- and (B) off-time CCDFs for EY on (black) glass and (red) TiO₂ substrates, presented with (dashed lines) the best fit to the data by lognormal distributions. CCDFs are derived from CPD analysis of 127 and 62 blinking traces on glass and TiO₂, respectively.

and MLE/KS analysis produces fit parameters that are sensitive to the substrate (see Table S2 in the Supporting Information). For example, statistically significant changes to μ and σ are observed for the on-time CCDFs of EY on glass (i.e., $\mu_{\rm on}$ = 0.5 \pm 0.1 and $\sigma_{\rm on}$ = 2.18 \pm 0.07) versus TiO₂ (i.e., $\mu_{\rm on}$ = -0.64 \pm 0.04 and $\sigma_{\rm on}$ = 1.52 \pm 0.02). The corresponding off-time CCDFs have similar μ_{off} values of approximately -0.2, but σ_{off} is substantially modified from 1.96 \pm 0.03 on glass to 2.43 \pm 0.08 on TiO₂. Altogether, the blinking behavior of EY is significantly altered on TiO₂ relative to glass. The emission intensity of EY is reduced in the presence of the semiconductor and many more blinking events are observed on TiO2 as compared to glass, consistent with an order of magnitude increase in $\langle v_{\text{event}} \rangle$ (i.e., from 0.03 s⁻¹ on glass to 0.3 s⁻¹ on TiO_2). At 20 s, the t_{on} of EY on glass is also much longer relative to TiO2, consistent with persistent emission from the dye in the absence of the semiconductor. The observation that the on- and off-time CCDFs of EY are best fit to lognormal distributions points to a common blinking mechanism for both substrates though the corresponding fit parameters are distinct.

Monte Carlo Simulations Based on the Albery Model. Previous single-molecule studies of rhodamines on glass and TiO₂ have shown that the observation of lognormally distributed on and off events is consistent with the so-called Albery model for dispersive electron transfer.²⁴ Albery and coworkers considered that the injection and BET dynamics on colloidal TiO2 exhibit heterogeneity due to local variations in the activation energy to photoinduced electron transfer $(\Delta G_{ii}^{\sharp})^{37}$ In this framework, the activation energies follow a Gaussian distribution according to $\Delta G_{ii}^{\ddagger} = (\Delta G_0^{\ddagger})_{ii} + \gamma x k_B T$, where i and j are the initial and final states, ΔG_0^{\ddagger} is the average activation energy, γ is the standard deviation of the energy distribution about ΔG_0^{\ddagger} , and the variations described by x are normally distributed. Substitution of this expression into the Arrhenius equation yields a dispersive rate constant, $k_{ii} = \kappa_{ii}$ $e^{-\gamma x}$, where κ_{ii} is a first-order rate constant derived from the average activation barrier (i.e., the ensemble median value; $\kappa_{ii} = e^{-(\Delta G_0^{\dagger})_{ij}/RT}$). Thus, the Albery model predicts that k_{ini} and k_{BET} are lognormally distributed. We note that the timedependent concentration of reactants is given by integrating the first-order rate law across the rate constant distribution to yield a Laplace transform of a lognormal function, which has no closed-form expression. Therefore, fitting the on- and offtime CCDFs to lognormal distributions is expected to report on the relative rate constants and extent of dispersion rather than absolute quantities. Indeed, our previous work has shown that the lognormal fit parameters $-\mu$ and σ are proportional to the average rate constant for electron transfer and kinetic dispersion, respectively.²⁵ These fit parameters can be compared across analogous systems (e.g., a series of xanthene dyes immobilized on the same substrate or one sensitizer across substrates).

In the context of the Albery model for dispersive electron transfer, the MLE/KS fitting results for EY demonstrate that injection to ${\rm TiO_2}$ occurs on faster timescales relative to glass as expected (i.e., $-\mu_{\rm on}$ is 0.64 ± 0.04 for ${\rm TiO_2}$ and -0.5 ± 0.1 for glass). The corresponding BET appears to occur on similar timescales (i.e., $-\mu_{\rm off}$ is 0.23 ± 0.04 and 0.2 ± 0.1 for EY on ${\rm TiO_2}$ and glass, respectively). The kinetic dispersion in both processes appears to be larger on glass relative to ${\rm TiO_2}$. Although this analysis reports on the relative rate constants and the extent of dispersion, the lognormal fit parameters themselves do not yield estimates of κ_{23} , κ_{31} , and γ . To quantify the timescales and better understand the kinetic dispersion that is operative in EY-sensitized ${\rm TiO_2}$, we performed a series of Monte Carlo simulations based on the Albery model.

The simulations are based on a simple three-level system comprising a (1) molecular ground state, (2) molecular excited state, and (3) non-emissive state due to electron transfer (Figure 5a). The rate constants for photoexcitation (k_{12}) and emission (k_{21}) are fixed input parameters that are estimated from the experimental laser power, the molecular extinction coefficient at 532 nm ($\varepsilon_{532} \sim 90,000~{\rm M}^{-1}~{\rm cm}^{-1}$ in ethanol), the diffraction-limited laser spot size, and the fluorescence lifetime of EY (i.e., 3.62 ns in ethanol). The population and depopulation of the non-emissive state occur with rate constants that vary in time according to the Albery model

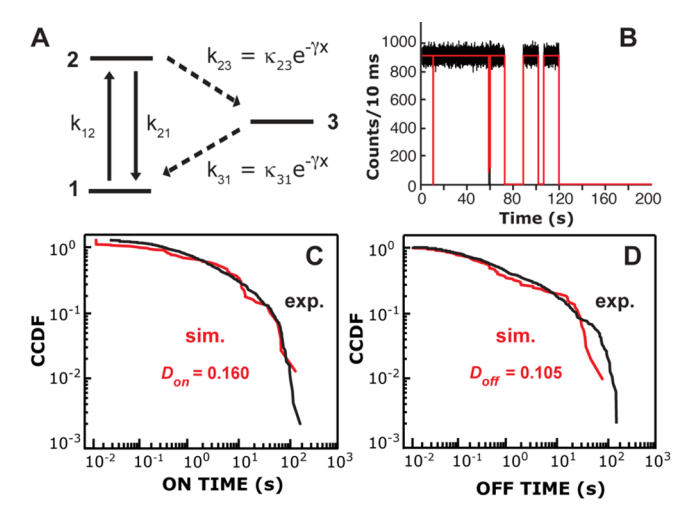


Figure 5. (A) Albery model for dispersive electron transfer employed in the Monte Carlo simulations where the rate constants of injection (k_{23}) and BET (k_{31}) are lognormally distributed. (B) Representative simulated blinking dynamics of EY on glass, obtained with $\kappa_{23}=10^3$ s⁻¹, $\kappa_{31}=10^{0.5}$ s⁻¹, $\gamma=3$ and 10 ms bin time shown with (red) CPD analysis. Corresponding (C) on- and (D) off-time CCDFs for (red) 20 simulated traces are in excellent agreement with the (black) experimental data, consistent with modest $D_{\rm on}$ and $D_{\rm off}$ values.

(i.e., $k_{ij} = \kappa_{ij} e^{-\gamma x}$). Single-molecule population trajectories are generated by comparing a uniformly distributed random number to the probability of leaving the occupied state (P_i) according to $P_i = \sum_j 1 - e^{-k_j t}$. A photon is added to the macroscopic 10 ms bin if the random number exceeds P_2 and the fluorescence quantum yield, $\Phi_f = k_{21}/(k_{21} + k_{23})$. Otherwise, the probability of dark-state population via dispersive electron transfer is tested. Consistent with prior Monte Carlo simulation studies, $^{24,25,62}_{ij}$ when simulations are run with only static variations in k_{ij} (i.e., each simulated molecule has a different, fixed κ_{ij}) the resulting emission trajectories are inconsistent with the empirical blinking dynamics. When γ is set to zero, the simulation yields simple first-order kinetics as expected.

These studies build on previous Monte Carlo simulations in several ways. First, prior studies have employed thresholding to analyze simulated blinking traces. ^{24,25} Although thresholding is straightforward to implement and relatively accurate in the context of first-order kinetics, it is known to produce spurious short-time events and assumes, rather than determines, the intensity-state distribution. To circumvent these issues, we analyzed the simulated blinking traces using the CPD algorithm for binned data. ^{47,49} Furthermore, parallelization of both CPD analysis and Monte Carlo simulations enabled us to reduce runtime and enhance scalability so that a large search space of the input parameters κ_{23} , κ_{31} , and γ could be tested. ⁴⁸

To model the blinking behavior of EY on glass, we performed a series of Monte Carlo simulations with k_{12} and k_{21} set to 9.34 \times 10⁴ and 2.76 \times 10⁸ s⁻¹, respectively, consistent with the experimental conditions. The median rate constants, κ_{23} and κ_{31} , were scanned from 10⁰ to 10⁶ s⁻¹ in half order-of-magnitude increments and the energetic dispersion value, γ , was varied from 1 to 5. For each unique set of input parameters, 20 blinking traces are simulated and analyzed with CPD to quantify the blinking metrics (i.e., $t_{\rm on}$, $t_{\rm off}$, and $\langle v_{\rm event} \rangle$), compile on- and off-time CCDFs, and determine the distance between the empirical and simulated CCDFs using a KS

Table 2. Simulated Blinking Metrics^a

$\kappa_{23} \ (s^{-1})$	$\kappa_{31} \ (s^{-1})$	γ	$\langle t_{\rm on} \rangle$ (s)	$\langle t_{\rm off} \rangle$ (s)	$\langle v_{ m event} \rangle \; ({ m s}^{-1})$	$D_{ m on}$	$D_{ m off}$	$D_{ m total}$
109	10^{3}	2.5	1.3 ± 0.3	0.4 ± 0.1	1.2 ± 0.2	0.227	0.400	0.627
10^{10}	5×10^{3}	2.0	3 ± 1	0.4 ± 0.1	0.6 ± 0.2	0.178	0.413	0.591
10^{10}	5×10^{3}	2.5	2.0 ± 0.9	1 ± 1	0.7 ± 0.2	0.247	0.245	0.492
10^{10}	5×10^{3}	3.0	1.7 ± 0.6	2.2 ± 0.4	0.5 ± 0.1	0.340	0.174	0.514
10^{10}	5×10^3	3.5	1.0 ± 0.9	4 ± 2	0.3 ± 0.1	0.457	0.074	0.531
10^{10}	10 ⁴	2.5	1.4 ± 0.3	0.46 ± 0.09	1.1 ± 0.2	0.200	0.392	0.592
10^{12}	10 ⁵	2.5	2 ± 7	30 ± 20	0.07 ± 0.05	0.548	0.387	0.935
experiment			2 ± 1	10 ± 10	0.3 ± 0.2	N/A	N/A	N/A

^aErrors correspond to standard deviation from the mean.

statistic (D). $D_{\rm on}$ and $D_{\rm off}$ are defined as the maximum distance between the empirical and simulated on- and off-time CCDFs, respectively, which can be summarized in a total KS statistic (i.e., $D_{\rm total} = D_{\rm on} + D_{\rm off}$). Since a perfect fit corresponds to $D_{\rm total} = 0$, the best simulations are determined by the set of input parameters that minimize $D_{\rm total}$ and the differences between the experimental and simulated blinking metrics.

Figure 5b shows a representative simulated blinking trace of EY on glass obtained using κ_{23} , κ_{31} , and γ set to 10^3 , $10^{0.5}$ s⁻¹, and 3, respectively. This simulation appears to capture the experimental blinking behavior (Figure 2d) though the intensities are higher than those observed experimentally, consistent with the <50% detection efficiency of the measurements. Furthermore, the blinking metrics collected from 20 simulations (i.e., $t_{\rm on}$ = 11.2 s, $t_{\rm off}$ = 10.3 s, and $\langle v_{\rm event} \rangle$ = 0.040 s⁻¹) are equivalent within error to the experimental data for EY on glass. Corresponding simulated CCDFs are presented in Figure 5c,d, which show excellent agreement to the experimental distributions, consistent with the smallest observed D_{total} value of 0.265 (see Figure S2 and Table S3 in the Supporting Information). Altogether, Monte Carlo simulations based on the Albery model can reproduce, both qualitatively and quantitively, the blinking dynamics of EY on glass.

Transitioning from glass to the semiconductor substrate, κ_{23} and κ_{31} are expected to be significantly faster on TiO₂, consistent with previous ensemble-averaged studies by Grätzel and co-workers who estimated $k_{\rm inj}$ and $k_{\rm BET}$ at 3.8 × 10¹² and 2 \times 10⁵ s⁻¹, respectively.^{39,45} Therefore, we performed Monte Carlo simulations of EY on TiO_2 with values of κ_{23} ranging from 10^8 to 10^{12} s⁻¹, κ_{31} from 10^2 to 10^6 s⁻¹, and γ between 1 and 5. Indeed, simulations outside this test region produced emission trajectories inconsistent with the experimental data (e.g., long-lived emission events or no emission at all). Table 2 summarizes the simulations that best represent the empirical data for EY on TiO2. Several simulations successfully reproduce one or more blinking metrics. For example, the set of simulations with κ_{23} , κ_{31} and γ set to 10^{12} s⁻¹, 10^5 s⁻¹, and 2.5, respectively, yield $t_{\rm on}$ and $t_{\rm off}$ values that match the experimental metrics. However, the corresponding $\langle v_{\rm event} \rangle$ is off by an order of magnitude and D_{total} is 0.935. These results highlight the practical advantage of performing simulations and CPD analyses in parallel, which enabled thousands of simulations to be completed and evaluated in the hours-todays' timeframe. In doing so, the search space could be quickly narrowed down to a smaller test region corresponding to κ_{23} ~ 10^{10} s⁻¹, $\kappa_{31} \sim 10^4$ s⁻¹, and $\gamma \sim 2.5$ (see Figure S3 in the Supporting Information).

Figure 6a shows a representative simulated blinking trace of EY on TiO₂ obtained using κ_{23} , κ_{31} , and γ values of 10¹⁰, 5 ×

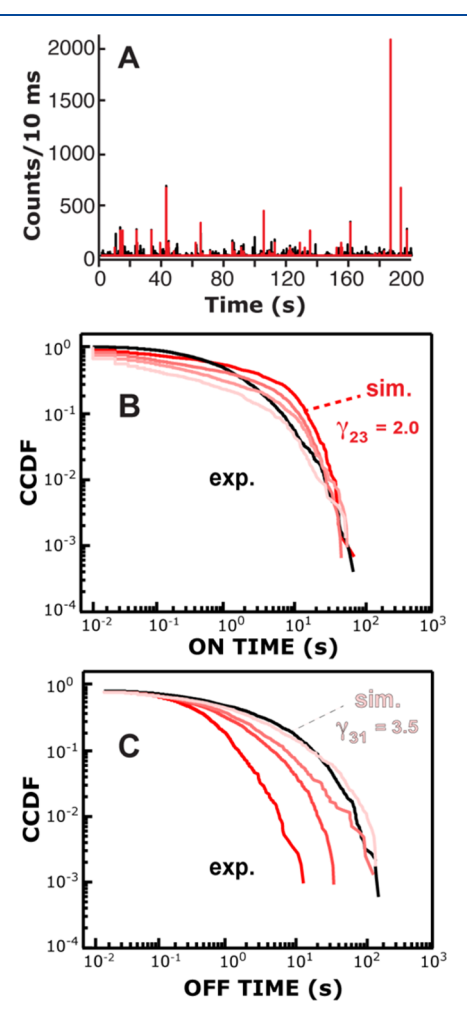


Figure 6. (A) Simulated blinking of EY on ${\rm TiO_2}$ obtained using $\kappa_{23}=10^{10}~{\rm s^{-1}}$, $\kappa_{31}=5\times10^3~{\rm s^{-1}}$, and $\gamma=2.5$ with (red) CPD analysis. (B) On- and (C) off-time CCDFs corresponding to (black) empirical and (red) simulated data as γ is increased in half increments from (red) 2.0 to (pink) 3.5.

 10^3 s⁻¹, and 2.5, respectively. The simulated trace is a good qualitative description of EY blinking on $\mathrm{TiO_2}$ (Figure 2b), which is quite distinct relative to the glass substrate. Corresponding blinking metrics collected from 100 simulations with these input parameters are $t_{\rm on} = 2.0$ s, $t_{\rm off} = 1.0$ s, and $\langle v_{\rm event} \rangle = 0.45 \, {\rm s}^{-1}$, equivalent within error to the empirical data. Furthermore, this simulation produced the smallest $D_{\rm total}$ of 0.492. This observation supports the interpretation that the blinking dynamics of EY on $\mathrm{TiO_2}$ are consistent with the Albery model for dispersive electron transfer, similar to previous findings for rhodamines on $\mathrm{TiO_2}^{2.5}$ Nonetheless,

some disparities between the experimental and simulated CCDFs remain. We observed that individual $D_{\rm on}$ and $D_{\rm off}$ values could be further optimized if the extent of energetic dispersion in the injection (γ_{23}) and BET (γ_{31}) processes is different.

Figure 6b shows the simulated on- and off-time CCDFs corresponding to $\kappa_{23} = 10^{10} \text{ s}^{-1}$ and $\kappa_{31} = 5 \times 10^3 \text{ s}^{-1}$, with γ values ranging from 2.0 to 3.5. As γ is increased, the simulated on-time CCDF is more divergent from the experimental distribution (i.e., D_{on} is increased from 0.178 to 0.457). However, the simulations at $\gamma = 3.5$ produce the best match to the experimental off-time CCDF, consistent with a minimized $D_{\rm off}$ value of 0.074. Taken together, Monte Carlo simulations with $\kappa_{23} = 10^{10} \text{ s}^{-1}$ and $\kappa_{31} = 5 \times 10^3 \text{ s}^{-1}$ best reproduce the blinking dynamics of EY on TiO₂. However, Table 2 demonstrates that there is some uncertainty in these values as similar input parameters (e.g., κ_{31} of 5 × 10³ s⁻¹ vs 10⁴ s⁻¹) produce comparable blinking metrics in terms of $t_{\rm on}$ and $t_{\rm off}$. These values are therefore considered to be order-ofmagnitude estimates. Energetic dispersion in the electron transfer processes is approximately 2.5 and the best match to the empirical data is achieved with $\gamma_{23} = 2.0$ and $\gamma_{31} = 3.5$. This means that in the context of the Albery model where x is drawn from a standard normal distribution, 99.7% of the k_{23} values fall between 2.5×10^7 and 4.0×10^{12} s⁻¹. These findings are consistent with a prior ensemble-averaged study that observed multiphasic injection kinetics from EY to TiO2 with a rough estimate of the fastest $k_{\rm inj}$ to be on the order of 10^{12} s⁻¹. The corresponding BET from TiO₂ is considerably slower, consistent with the literature, ³⁹ with most k_{31} values spanning 0.14 to $1.8 \times 10^8 \text{ s}^{-1}$.

Ultimately, Monte Carlo simulations based on the Albery model successfully reproduce the blinking behavior of EY and provide for quantification of the dispersive kinetics occurring in the system. Importantly, this is accomplished with a simple three-level system for dispersive electron transfer without the need to include injection from T_1 . Therefore, our Monte Carlo simulations support the interpretation that the blinking of EY on ${\rm TiO}_2$ occurs due to injection from S_1 and the corresponding BET to repopulate S_0 . This observation suggests that injection from multiple excited states (both S_1 and T_1) does not appreciably contribute to the dispersive electron transfer kinetics of EY on ${\rm TiO}_2$ and instead points to environmental origins.

Environmental versus Photophysical Origins of Kinetic Dispersion. To further test the hypothesis that kinetic dispersion in EY-sensitized TiO_2 is predominately governed by environmental, not photophysical, heterogeneity, we examined the blinking behavior of EY alongside R123 and SROX, which do not possess heavy atoms and inject only from S₁ (Figure 1, $^1\text{R}123^{*/+} = -1.13 \text{ V}$ and $^1\text{SROX}^{*/+} = -0.81 \text{ V}$ vs NHE). The blinking dynamics of 98 and 146 molecules of R123 and SROX on TiO_2 , respectively, were recorded and analyzed using CPD. Blinking statistics for R123 and SROX are shown in Table S4 of the Supporting Information. Figure 7a,b presents the on- and off-time CCDFs of EY, R123, and SROX on TiO_2 , with corresponding best fits to lognormal distributions as determined by the MLE/KS method.

The fit parameters of the on-time CCDFs are distinct for EY (i.e., $-\mu_{\rm on} = 0.64 \pm 0.03$ and $\sigma_{\rm on} = 1.52 \pm 0.02$) versus R123 and 5ROX (i.e., $-\mu_{\rm on} \sim 0.3 \pm 0.1$ and $\sigma_{\rm on} \sim 1.63 \pm 0.07$). These results demonstrate that the injection of EY to TiO₂ occurs on faster timescales and with somewhat less kinetic

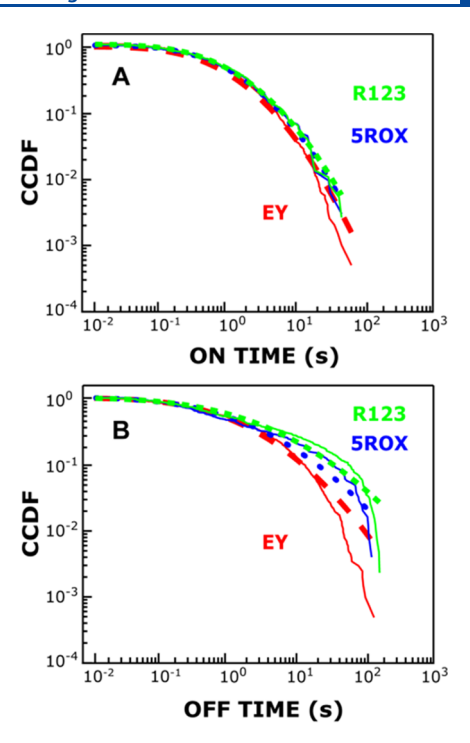


Figure 7. (A) On- and (B) off-time CCDFs for EY, R123, and 5ROX on TiO_2 , presented with best fits to lognormal functions (EY = red, dashed; R123 = green, squares; 5ROX = blue, circles).

dispersion relative to R123 and 5ROX. That is, when access to the T₁ state is minimized in going from EY to R123 and 5ROX, kinetic dispersion is actually increased. These changes are even more dramatic for the off-time CCDFs, where the fit parameters are significantly modified from $-\mu_{\rm off}$ = 0.23 \pm 0.04 and $\sigma_{\rm off}$ = 1.96 \pm 0.03 for EY to $-\mu_{\rm off}$ = 0.0 \pm 0.1 and $\sigma_{\rm off}$ = 2.4 \pm 0.1 for 5ROX and $-\mu_{\rm off}$ = -0.3 ± 0.1 and $\sigma_{\rm off}$ = 2.44 \pm 0.09 for R123. Therefore, BET is faster and considerably less dispersive for EY on TiO₂ as compared to the rhodamines. The observation that EY exhibits less kinetic dispersion in both the injection and BET dynamics relative to the rhodamines is consistent with the Monte Carlo simulation results, which successfully modeled the blinking of EY using a three-level system involving injection only from S₁. Collectively, these results support the interpretation that environmental heterogeneity, not electron transfer from both S_1 and T_1 states, is predominately responsible for kinetic dispersion at the EY-TiO₂ interface.

To determine the physical origin of these environmental inhomogeneities, we considered the Albery model within the framework of the Marcus–Gerisher theory for interfacial electron transfer. ^{10,11,63} In the Marcus–Gerischer theory, the discrete states of an adsorbed dye sensitizer [W(E), eq 1] can be expressed in terms of ΔG_0^{\ddagger} , the driving force (ΔG^0) , and the reorganization energy (λ) .

$$W(E) = \frac{1}{\sqrt{4\pi\lambda k_{\rm B}T}} \exp\left(\frac{-\Delta G_0^{\ddagger}}{k_{\rm B}T}\right)$$
$$= \frac{1}{\sqrt{4\pi\lambda k_{\rm B}T}} \exp\left(\frac{-\left[\Delta G^0(E) + \lambda\right]^2}{4\lambda k_{\rm B}T}\right) \tag{1}$$

$$k_{\rm ET} \propto \int V^2 (1 - f(E, E_{\rm f})) g(E) W(E) dE$$
 (2)

In this formalism, the rate constant for electron transfer ($k_{\rm ev}$ eq 2) is determined by the electronic coupling between states (V) and the energetic overlap between W(E) and the exponentially distributed density of semiconductor states [$g(E) \propto {\rm e}^{-E/E_0}$]. $f(E,E_{\rm f})$ is a Fermi-Dirac term that accounts for the electronic occupancy of the semiconductor. It is important to note that the Marcus—Gerischer theory yields a single $k_{\rm ev}$ which is inconsistent with the observation of dispersive electron transfer kinetics as is the case for EY-sensitized TiO₂. To account for kinetic dispersion, we must consider the variations in V, W(E), and g(E) that may be operative.

Previous studies by Lian and co-workers demonstrated that the multiphasic injection kinetics of $\operatorname{Ru}(\operatorname{dcbpy})_2(\operatorname{SCN})_2$ -sensitized ZnO could be modeled using a Gaussian distribution of electronic coupling between the π^* orbital of the Ru N3 dcbpy ligand and the accepting orbital in the semiconductor. However, a Gaussian distribution of V is inconsistent with the observation of lognormal distributions predicted by the Albery model. Furthermore, Tachibana et al. demonstrated that heterogeneity in V cannot alone be responsible for the broad range of injection timescales observed on anatase nanocrystalline TiO_2 films. Therefore, although inhomogeneities in V at the $\operatorname{EY-TiO}_2$ interface are probable, they are unlikely to govern the observed kinetic dispersion.

In their original paper, Albery and co-workers considered the lognormal distributions of $k_{\rm et}$ to arise from site-to-site variations in ΔG_0^{\ddagger} that occur due to a distribution of TiO₂ particle sizes and surface charges. More recently, Durrant and co-workers modeled the non-exponential injection kinetics of Zn porphyrin and Ru(II) complexes on TiO_2 by considering variations in $g(E) \propto e^{-E/\tilde{E}_0}$, which occur from local inhomogeneities in size, charge, and defect density on the TiO₂ surface. 13,19 We note that their approach is mathematically equivalent to Albery's model. In other words, the Albery model is a simple framework to account for energetic fluctuations at the dye-semiconductor interface arising from relative shifts of either the dye [W(E)] or semiconductor states [g(E)]. As such, we can utilize the simulation results to estimate the extent of energetic dispersion. Monte Carlo simulations employing an energy distribution with a standard deviation of ~2.5 best reproduced the empirical data for EY on TiO_2 , with individual values corresponding to $\gamma_{23} = 2.0$ and γ_{31} = 3.5. Therefore, the energetic fluctuations relative to the reported E_0 values for TiO_2 (i.e., ~100 meV)⁶⁴ are approximately 200 and 350 meV for the injection and BET processes, respectively. Energetic dispersion on the order of hundreds of meV is consistent with prior studies of inorganic sensitizers on $TiO_2^{13,19}$ which was attributed to static (i.e., site-to-site) variations across the sample.

To examine the physical origin of these energy fluctuations, the contributions from both static and dynamic inhomogeneities at the EY–TiO₂ interface must be considered. Prior studies have shown that site-to-site variations in particle radii, surface charge, crystal faces, defect density, and binding site are present across anatase nanocrystalline TiO₂ films, which can yield significant shifts in the relative energies of g(E) and W(E). While some local variations are surely present within the sintered anatase films employed in this study, our Monte Carlo simulations require dynamic fluctuations (i.e., changes to $k_{\rm ET}$ at one site with time) to reproduce the empirical blinking behavior of EY. Dynamic

variations in g(E) seem unlikely since the measurements are taken in the absence of a solvent/electrolyte system. However, dynamic fluctuations in W(E) via vibrational motion or changes in binding configuration may be operative. For example, Zhang et al. demonstrated that the hydrogen-bonded monodentate and bidentate bridging adsorption geometries of EY on TiO_2 , which are separated in energy by ~100 meV, can be manipulated by adding a small amount of water.⁶⁶ Thus, small quantities of adsorbed water at the dye-TiO₂ interface may result in dynamic changes to the binding configuration and W(E). Our observation that the faster injection process is less dispersive relative to BET may be a consequence of less residence time in the molecular excited state for such dynamic fluctuations to occur. The presence of interfacial water would also influence the reorganization energy and coupling between the excited and charge-separated states though the observation of lognormal distributions suggests that these factors do not drive the kinetic dispersion. Ultimately, by probing EYsensitized TiO2 one molecule at a time, we find that kinetic dispersion is substantial, varying by 5 to 8 orders of magnitude in time and governed by both static and dynamic inhomogeneities at the dye-semiconductor interface and not injection from multiple excited states. It would be interesting to further study the static disorder and dynamic fluctuations (e.g., through single-molecule measurements on rutile and anatase single crystals or covalent attachment of EY to TiO2 via phosphonic-acid linkages) though such measurements are beyond the scope of the present study.

CONCLUSIONS

Elucidating the extent and origin of kinetic dispersion at the dye-semiconductor interface is important for the future optimization of DSSCs and DSPECs. By removing the effects of ensemble averaging and molecular aggregation, we untangled the various factors that contribute to kinetic dispersion in EY-sensitized TiO2, specifically focusing on sample heterogeneity versus competition between injection and excited-state relaxation. Single-molecule blinking measurements reveal that the on- and off-time CCDFs for EY on TiO₂ are best represented by lognormal distributions, with fit parameters that are sensitive to the substrate and the sensitizer. We show using Monte Carlo simulations that the observation of lognormal distributions is consistent with the Albery model for dispersive electron transfer, where energy fluctuations at the dye-semiconductor interface that arise from relative shifts of either the dye or semiconductor states are normally distributed. By studying two rhodamine sensitizers that do not possess heavy atoms and inject only from S1, we demonstrate that competition between injection and intersystem crossing to T₁ does not govern the kinetic dispersion of EY. Indeed, Monte Carlo simulations based on the Albery model, with injection occurring from S₁, successfully reproduce the blinking behavior of EY on TiO_2 using a median k_{ini} of $\sim 10^{10}$ s⁻¹, $k_{\rm BET}$ of $\sim 10^4$ s⁻¹, and a corresponding energetic dispersion of ~200-350 meV. Although site-to-site variations across the nanocrystalline TiO2 film certainly contribute to this energetic dispersion, our results suggest that dynamic fluctuations in binding configuration and/or vibrational motion play a decisive role. Collectively, this study reveals the tremendous static and dynamic inhomogeneities present at the dye-TiO₂ interface even without the presence of a redox mediator or catalyst for chemical fuel generation. This molecular-level study highlights some of the fundamental

limitations to minimizing unwanted kinetic dispersion and motivates further investigations of covalently attached photosensitizers in the presence and absence of a supporting electrolyte.

ASSOCIATED CONTENT

Supporting Information

The Supporting Information is available free of charge at https://pubs.acs.org/doi/10.1021/acs.jpcc.1c07597.

Details on the CPD algorithm for binned data, additional blinking statistics for EY on glass and R123 and 5ROX on TiO₂, and additional Monte Carlo simulation results for EY on glass and TiO₂ (PDF) Critical values for binned data (TXT)

AUTHOR INFORMATION

Corresponding Author

Kristin L. Wustholz — Department of Chemistry, College of William & Mary, Williamsburg, Virginia 23187, United States; Occid.org/0000-0001-7705-4240; Email: kwustholz@wm.edu

Authors

Kelly M. Kopera – Department of Chemistry, College of William & Mary, Williamsburg, Virginia 23187, United States

Harrison G. Tuckman – Department of Chemistry, College of William & Mary, Williamsburg, Virginia 23187, United States

Grayson R. Hoy – Department of Chemistry, College of William & Mary, Williamsburg, Virginia 23187, United States

Complete contact information is available at: https://pubs.acs.org/10.1021/acs.jpcc.1c07597

Author Contributions

The manuscript was written through contributions of all authors. All authors have given approval to the final version of the manuscript.

Notes

The authors declare no competing financial interest.

ACKNOWLEDGMENTS

The experimental work was supported by a grant from the National Science Foundation (CHE-1664828). The simulation studies were supported by the National Science Foundation (CHE-2102099). K.M.K. acknowledges the Virginia Space Grant Consortium (VSGC) for support through a NASA VSGC Undergraduate Research Scholarship. G.R.H. acknowledges the Charles Center at William & Mary for a summer research scholarship. The authors acknowledge William & Mary Research Computing for providing computational resources and/or technical support that have contributed to the results reported within this paper. URL: https://www.wm.edu/it/rc.

REFERENCES

- (1) O'Regan, B.; Grätzel, M. A Low-Cost, High-Efficiency Solar Cell Based on Dye-Sensitized Colloidal TiO₂ Films Brian. *Nature* **1991**, 353, 737–740.
- (2) Hagfeldt, A.; Boschloo, G.; Sun, L.; Kloo, L.; Pettersson, H. Dye-Sensitized Solar Cells. *Chem. Rev.* **2010**, *110*, 6595–6663.

- (3) Banin, U.; Waiskopf, N.; Hammarström, L.; Boschloo, G.; Freitag, M.; Johansson, E. M. J.; Sá, J.; Tian, H.; Johnston, M. B.; Herz, L. M.; et al. Nanotechnology for Catalysis and Solar Energy Conversion. *Nanotechnology* **2021**, *32*, 042003.
- (4) Grätzel, M. Photoelectrochemical Cells. *Nature* **2001**, 414, 338–344
- (5) Concepcion, J. J.; House, R. L.; Papanikolas, J. M.; Meyer, T. J. Chemical Approaches to Artificial Photosynthesis. *Proc. Natl. Acad. Sci. U.S.A.* 2012, 109, 15560–15564.
- (6) Willkomm, J.; Orchard, K. L.; Reynal, A.; Pastor, E.; Durrant, J. R.; Reisner, E. Dye-Sensitised Semiconductors Modified with Molecular Catalysts for Light-Driven H₂ Production. *Chem. Soc. Rev.* **2016**, *45*, 9–23.
- (7) Katoh, R.; Furube, A.; Yoshihara, T.; Hara, K.; Fujihashi, G.; Takano, S.; Murata, S.; Arakawa, H.; Tachiya, M. Efficiencies of Electron Injection from Excited N3 Dye into Nanocrystalline Semiconductor (ZrO₂, TiO₂, ZnO, Nb₂O₅, SnO₂, In₂O₃) Films. *J. Phys. Chem. B* **2004**, *108*, 4818–4822.
- (8) Ardo, S.; Meyer, G. J. Photodriven Heterogeneous Charge Transfer with Transition-Metal Compounds Anchored to TiO₂ Semiconductor Surfaces. *Chem. Soc. Rev.* **2009**, *38*, 115–164.
- (9) Jin, S.; Lian, T. Electron Transfer Dynamics from Single CdSe/ZnS Quantum Dots to TiO₂ Nanoparticles. *Nano Lett.* **2009**, 9, 2448–2454.
- (10) Listorti, A.; O'Regan, B.; Durrant, J. R. Electron Transfer Dynamics in Dye-Sensitized Solar Cells. *Chem. Mater.* **2011**, 23, 3381–3399.
- (11) Bangle, R. E.; Meyer, G. J. Factors That Control the Direction of Excited-State Electron Transfer at Dye-Sensitized Oxide Interfaces. *J. Phys. Chem. C* **2019**, *123*, 25967–25976.
- (12) Asbury, J. B.; Wang, Y.; Lian, T. Multiple-Exponential Electron Injection in Ru(Dcbpy)₂(SCN)₂ Sensitized ZnO Nanocrystalline Thin Films. *J. Phys. Chem. B* **1999**, *103*, 6643–6647.
- (13) Tachibana, Y.; Rubtsov, I. V.; Montanari, I.; Yoshihara, K.; Klug, D. R.; Durrant, J. R. Transient Luminescence Studies of Electron Injection in Dye Sensitised Nanocrystalline TiO₂ Films. *J. Photochem. Photobiol., A* **2001**, *142*, 215–220.
- (14) Walters, K. A.; Gaal, D. A.; Hupp, J. T. Interfacial Charge Transfer and Colloidal Semiconductor Dye-Sensitization: Mechanism Assessment via Stark Emission Spectroscopy. *J. Phys. Chem. B* **2002**, *106*, 5139–5142.
- (15) Bisquert, J.; Zaban, A.; Greenshtein, M.; Mora-Seró, I. Determination of Rate Constants for Charge Transfer and the Distribution of Semiconductor and Electrolyte Electronic Energy Levels in Dye-Sensitized Solar Cells by Open-Circuit Photovoltage Decay Method. J. Am. Chem. Soc. 2004, 126, 13550–13559.
- (16) Tachibana, Y.; Nazeeruddin, M. K.; Grätzel, M.; Klug, D. R.; Durrant, J. R. Electron Injection Kinetics for the Nanocrystalline TiO2films Sensitised with the Dye (Bu4N)₂Ru(DcbpyH)₂(NCS)₂. *Chem. Phys.* **2002**, 285, 127–132.
- (17) Katoh, R.; Furube, A.; Barzykin, A. V.; Arakawa, H.; Tachiya, M. Kinetics and Mechanism of Electron Injection and Charge Recombination in Dye-Sensitized Nanocrystalline Semiconductors. *Coord. Chem. Rev.* **2004**, 248, 1195–1213.
- (18) Wenger, B.; Grätzel, M.; Moser, J.-E. Rationale for Kinetic Heterogeneity of Ultrafast Light-Induced Electron Transfer from Ru(II) Complex Sensitizers to Nanocrystalline TiO₂. *J. Am. Chem. Soc.* **2005**, *127*, 12150–12151.
- (19) Koops, S. E.; Durrant, J. R. Transient Emission Studies of Electron Injection in Dye Sensitised Solar Cells. *Inorg. Chim. Acta* **2008**, *361*, 663–670.
- (20) Zigler, D. F.; Morseth, Z. A.; Wang, L.; Ashford, D. L.; Brennaman, M. K.; Grumstrup, E. M.; Brigham, E. C.; Gish, M. K.; Dillon, R. J.; Alibabaei, L.; et al. Disentangling the Physical Processes Responsible for the Kinetic Complexity in Interfacial Electron Transfer of Excited Ru(II) Polypyridyl Dyes on TiO₂. *J. Am. Chem. Soc.* **2016**, *138*, 4426–4438.
- (21) Guo, L.; Wang, Y.; Lu, H. P. Combined Single-Molecule Photon-Stamping Spectroscopy and Femtosecond Transient Absorp-

- tion Spectroscopy Studies of Interfacial Electron Transfer Dynamics. *J. Am. Chem. Soc.* **2010**, *132*, 1999–2004.
- (22) Biju, V.; Micic, M.; Hu, D.; Lu, H. P. Intermittent Single-Molecule Interfacial Electron Transfer Dynamics. *J. Am. Chem. Soc.* **2004**, *126*, 9374–9381.
- (23) Govind Rao, V.; Lu, H. P. Inhomogeneous and Complex Interfacial Electron-Transfer Dynamics: A Single-Molecule Perspective. *ACS Energy Lett.* **2016**, *1*, 773–791.
- (24) Wong, N. Z.; Ogata, A. F.; Wustholz, K. L. Dispersive Electron-Transfer Kinetics from Single Molecules on TiO₂ Nanoparticle Films. *J. Phys. Chem. C* **2013**, *117*, 21075–21085.
- (25) Tan, J. A.; Rose, J. T.; Cassidy, J. P.; Rohatgi, S. K.; Wustholz, K. L. Dispersive Electron-Transfer Kinetics of Rhodamines on TiO₂: Impact of Structure and Driving Force on Single-Molecule Photophysics. *J. Phys. Chem. C* **2016**, *120*, 20710–20720.
- (26) Tachikawa, T.; Majima, T. Single-Molecule Fluorescence Imaging of ${\rm TiO_2}$ Photocatalytic Reactions. *Langmuir* **2009**, 25, 7791–7802.
- (27) Moerner, W. E.; Orrit, M. Illuminating Single Molecules in Condensed Matter. *Science* **1999**, 283, 1670–1676.
- (28) Wu, X.; Bell, T. D. M.; Yeow, E. K. L. Electron Transport in the Long-Range Charge-Recombination Dynamics of Single Encapsulated Dye Molecules on TiO₂ Nanoparticle Films. *Angew. Chem., Int. Ed.* **2009**, *48*, 7379–7382.
- (29) Mitsui, M.; Unno, A.; Mori, K. Methodology for Discriminating between Competitive Photophysical Processes in Photoblinking: Application to the Fluorescence Blinking of Single Dye Molecules Adsorbed on TiO₂. Chem. Lett. **2017**, 46, 866–869.
- (30) Wang, Y.; Wang, X.; Lu, H. P. Probing Single-Molecule Interfacial Geminate Electron—Cation Recombination Dynamics. *J. Am. Chem. Soc.* **2009**, *131*, 9020—9025.
- (31) McNeil, I. J.; Ashford, D. L.; Luo, H.; Fecko, C. J. Power-Law Kinetics in the Photoluminescence of Dye-Sensitized Nanoparticle Films: Implications for Electron Injection and Charge Transport. *J. Phys. Chem. C* **2012**, *116*, 15888–15899.
- (32) McNeil, I. J.; Alibabaei, L.; Ashford, D. L.; Fecko, C. J. Investigation of Factors That Affect Excited-State Lifetime Distribution of Dye-Sensitized Nanoparticle Films. *J. Phys. Chem. C* **2013**, *117*, 17412–17420.
- (33) Chen, W.-C.; Marcus, R. A. Theory of a Single Dye Molecule Blinking with a Diffusion-Based Power Law Distribution. *J. Phys. Chem. C* **2012**, *116*, 15782–15789.
- (34) Riley, E. A.; Hess, C. M.; Whitham, P. J.; Reid, P. J. Beyond Power Laws: A New Approach for Analyzing Single Molecule Photoluminescence Intermittency. *J. Chem. Phys.* **2012**, *136*, 184508.
- (35) Mitsui, M.; Fukui, H.; Takahashi, R.; Takakura, Y.; Mizukami, T. Single-Molecule Fluorescence Spectroscopy of Perylene Diimide Dyes in a γ -Cyclodextrin Film: Manifestation of Photoinduced H-Atom Transfer via Higher Triplet (n, π^*) Excited States. *J. Phys. Chem. A* **2017**, *121*, 1577–1586.
- (36) Grollman, R.; Quist, N.; Robertson, A.; Rath, J.; Purushothaman, B.; Haley, M. M.; Anthony, J. E.; Ostroverkhova, O. Single-Molecule Level Insight into Nanoscale Environment-Dependent Photophysics in Blends. *J. Phys. Chem. C* **2017**, *121*, 12483–12494.
- (37) Albery, W. J.; Bartlett, P. N.; Wilde, C. P.; Darwent, J. R. A General Model for Dispersed Kinetics in Heterogeneous Systems. *J. Am. Chem. Soc.* **1985**, *107*, 1854–1858.
- (38) Lazarides, T.; McCormick, T.; Du, P.; Luo, G.; Lindley, B.; Eisenberg, R. Making Hydrogen from Water Using a Homogeneous System Without Noble Metals. *J. Am. Chem. Soc.* **2009**, *131*, 9192–9194.
- (39) Moser, J.; Grätzel, M. Photosensitized Electron Injection in Colloidal Semiconductors. J. Am. Chem. Soc. 1984, 106, 6557–6564.
- (40) Wang, J.; Liu, Y.; Li, Y.; Xia, L.; Jiang, M.; Wu, P. Highly Efficient Visible-Light-Driven H₂ Production via an Eosin Y-Based Metal-Organic Framework. *Inorg. Chem.* **2018**, *57*, 7495–7498.

- (41) Hartley, C. L.; Dirisio, R. J.; Screen, M. E.; Mayer, K. J.; McNamara, W. R. Iron Polypyridyl Complexes for Photocatalytic Hydrogen Generation. *Inorg. Chem.* **2016**, *55*, 8865–8870.
- (42) Penzkofer, A.; Beidoun, A.; Daiber, M. Intersystem-Crossing and Excited-State Absorption in Eosin Y Solutions Determined by Picosecond Double Pulse Transient Absorption Measurements. *J. Lumin.* 1992, *51*, 297–314.
- (43) Redmond, G.; Fitzmaurice, D. Spectroscopic Determination of Flatband Potentials for Polycrystalline Titania Electrodes in Nonaqueous Solvents. *J. Phys. Chem.* **1993**, *97*, 1426–1430.
- (44) Fabregat-Santiago, F.; Mora-Seró, I.; Garcia-Belmonte, G.; Bisquert, J. Cyclic Voltammetry Studies of Nanoporous Semi-conductors. Capacitive and Reactive Properties of Nanocrystalline TiO₂ Electrodes in Aqueous Electrolyte. *J. Phys. Chem. B* **2003**, *107*, 758–768.
- (45) Pelet, S.; Grätzel, M.; Moser, J.-E. Femtosecond Dynamics of Interfacial and Intermolecular Electron Transfer at Eosin-Sensitized Metal Oxide Nanoparticles. *J. Phys. Chem. B* **2003**, *107*, 3215–3224.
- (46) Shen, T.; Zhao, Z.-G.; Yu, Q.; Xu, H.-J. Photosensitized Reduction of Benzil by Heteroatom-Containing Anthracene Dyes. *J. Photochem. Photobiol., A* **1989**, 47, 203–212.
- (47) Watkins, L. P.; Yang, H. Detection of Intensity Change Points in Time-Resolved Single-Molecule Measurements. *J. Phys. Chem. B* **2005**, *109*, 617–628.
- (48) Song, N.; Yang, H. Parallelization of Change Point Detection. *J. Phys. Chem. A* **2017**, *121*, 5100–5109.
- (49) Boudjellaba, H.; MacGibbon, B.; Sawyer, P. On Exact Inference for Change in a Poisson Sequence. *Commun. Stat.* **2001**, *30*, 407–434.
- (50) Tan, J. A.; Garakyaraghi, S.; Tagami, K. A.; Frano, K. A.; Crockett, H. M.; Ogata, A. F.; Patterson, J. D.; Wustholz, K. L. Contributions from Excited-State Proton and Electron Transfer to the Blinking and Photobleaching Dynamics of Alizarin and Purpurin. *J. Phys. Chem. C* **2017**, *121*, 97–106.
- (51) Wustholz, K. L.; Bott, E. D.; Kahr, B.; Reid, P. J. Memory and Spectral Diffusion in Single-Molecule Emission. *J. Phys. Chem. C* **2008**, *112*, 7877–7885.
- (52) Crouch, C. H.; Sauter, O.; Wu, X.; Purcell, R.; Querner, C.; Drndic, M.; Pelton, M. Facts and Artifacts in the Blinking Statistics of Semiconductor Nanocrystals. *Nano Lett.* **2010**, *10*, 1692–1698.
- (53) Riley, E. A.; Hess, C. M.; Pioquinto, J. R. L.; Kaminsky, W.; Kahr, B.; Reid, P. J. Proton Transfer and Photoluminescence Intermittency of Single Emitters in Dyed Crystals. *J. Phys. Chem. B* **2013**, *117*, 4313–4324.
- (54) Nishimura, Y.; Sakuragi, H.; Tokumaru, K. Xanthene Dye-Sensitized Electron Transfer to Methylviologen in Aqueous Organic Solution. Effects of Organic Solvents and Heavy Atoms in the Dyes. *Bull. Chem. Soc. Ipn.* **1992**, *65*, 2887–2893.
- (55) Garland, P. B.; Moore, C. H. Phosphorescence of protein-bound eosin and erythrosin. A possible probe for measurements of slow rotational mobility. *Biochem. J.* 1979, 183, 561–572.
- (56) Levin, P. P.; Costa, S. M. B. Kinetics of Oxygen Induced Delayed Fluorescence of Eosin Adsorbed on Alumina. the Dependence on Dye and Oxygen Concentrations. *Chem. Phys. Lett.* **2000**, 320, 194–201.
- (57) Lynch, P. G.; Richards, H.; Wustholz, K. L. Unraveling the Excited-State Dynamics of Eosin y Photosensitizers Using Single-Molecule Spectroscopy. *J. Phys. Chem. A* **2019**, 123, 2592–2600.
- (58) Mitsui, M.; Unno, A.; Azechi, S. Understanding Photoinduced Charge Transfer Dynamics of Single Perylenediimide Dyes in a Polymer Matrix by Bin-Time Dependence of Their Fluorescence Blinking Statistics. *J. Phys. Chem. C* **2016**, *120*, 15070–15081.
- (59) Clauset, A.; Shalizi, C. R.; Newman, M. E. J. Power-Law Distributions in Empirical Data. *SIAM Rev.* **2009**, *51*, 661–703.
- (60) Virkar, Y.; Clauset, A. Power-Law Distributions in Binned Empirical Data. *Ann. Appl. Stat.* **2014**, *8*, 89–119.
- (61) Fleming, G. R.; Knight, A. W. E.; Morris, J. M.; Morrison, R. J. S.; Robinson, G. W. Picosecond Fluorescence Studies of Xanthene Dyes. J. Am. Chem. Soc. 2002, 99, 4306–4311.

- (62) Yeow, E. K. L.; Melnikov, S. M.; Bell, T. D. M.; De Schryver, F. C.; Hofkens, J. Characterizing the Fluorescence Intermittency and Photobleaching Kinetics of Dye Molecules Immobilized on a Glass Surface. *J. Phys. Chem. A* **2006**, *110*, 1726–1734.
- (63) Gerischer, H. Charge transfer processes at semiconductorelectrolyte interfaces in connection with problems of catalysis. *Surf. Sci.* **1969**, *18*, 97–122.
- (64) Durrant, J. R.; Haque, S. A.; Palomares, E. Towards Optimisation of Electron Transfer Processes in Dye Sensitised Solar Cells. *Coord. Chem. Rev.* **2004**, 248, 1247–1257.
- (65) Jin, S.; Martinson, A. B. F.; Wiederrecht, G. P. Reduced Heterogeneity of Electron Transfer into Polycrystalline TiO₂ Films: Site Specific Kinetics Revealed by Single-Particle Spectroscopy. *J. Phys. Chem. C* **2012**, *116*, 3097–3104.
- (66) Zhang, F.; Shi, F.; Ma, W.; Gao, F.; Jiao, Y.; Li, H.; Wang, J.; Shan, X.; Lu, X.; Meng, S. Controlling Adsorption Structure of Eosin Y Dye on Nanocrystalline TiO₂ Films for Improved Photovoltaic Performances. J. Phys. Chem. C 2013, 117, 14659–14666.